Research Square

Preprints are preliminary reports that have not undergone peer review.
They should not be considered conclusive, used to inform clinical practice,
or referenced by the media as validated information.

Hydrological Drought Risk Assessment and Management Prioritization under Changing Climate: Part 1. Scenario-Neutral Assessment of Bivariate Drought Hazard

Jiyoung Kim
Hanyang University - ERICA Campus
Tae-Woong Kim
twkim72@hanyang.ac.kr

Hanyang University - ERICA Campus https://orcid.org/0000-0002-1793-2483

Research Article

Keywords: Hydrological drought, Bivariate drought frequency analysis, Scenario-neutral approach, Climate change impact assessment

Posted Date: October 29th, 2026

DOI: https://doi.org/10.21203/rs.3.rs-11135473/v1

License: This work is licensed under a Creative Commons Attribution 4.0 International License.
Read Full License

Hydrological Drought Risk Assessment and Management Prioritization under Changing Climate: Part 1. Scenario-Neutral Assessment of Bivariate Drought Hazard

Jiyoung Kim [1], Tae-Woong Kim [2]

[1] Ph.D. Candidate, Department of Smart City Engineering, Hanyang University, Seoul, Korea. ORCID: https://orcid.org/0009-0009-0931-0957

[2] Professor, Department of Civil and Environmental Engineering, Hanyang University ERICA, Ansan, Korea. ORCID: https://orcid.org/0000-0002-1793-2483

Corresponding author: Tae-Woong Kim (e-mail: twkim72@hanyang.ac.kr)

Abstract

The results of a climate change impact assessment can differ substantially depending on the choice of climate change scenario and climate model. This study introduced a scenario-neutral approach that does not depend on specific future projections and evaluated the hydrological drought hazard of the 113 middle-sized watersheds of South Korea across a precipitation-temperature exposure space defined by systematic perturbations in precipitation and temperature. The design drought return period was estimated by copula-based bivariate frequency analysis of drought duration and severity applied to the simulated daily streamflow for 1974-2025, and watershed-specific response surfaces were constructed from 252 precipitation-temperature perturbation combinations (R^2=0.568-0.932). Local sensitivity analysis around the baseline point showed that the return

period increased with increasing precipitation and decreased with rising temperature, and the national median precipitation increase required to offset 1℃ of warming was 2.64%. When the 72 projections from 18 general circulation models (GCMs) under 4 Shared Socioeconomic Pathway (SSP) scenarios were mapped onto the response surfaces, the ensemble median showed an increase in the return period for all SSP-period combinations, whereas 13.5-31.3% of the individual projections showed a decrease, identifying unfavorable projections that run counter to the central tendency. These results show that the scenario-neutral response surfaces allow changes in drought hazard under diverse future projections to be compared on a consistent basis, and they provide the hazard information for the watershed-level management prioritization.

Keywords: Hydrological drought, Bivariate drought frequency analysis, Scenario-neutral approach, Climate change impact assessment

1 Introduction

Since the mid-twentieth century, climate change has intensified the hydrological cycle and altered precipitation-evapotranspiration regimes, increasing the spatio-temporal variability of water availability. These changes have also increased the occurrence of hydroclimatic extremes, including floods and droughts (IPCC 2023; Konapala et al. 2020; Ficklin et al. 2022). Drought, unlike floods, lacks a clearly identifiable onset and termination and its impacts unfold over long periods and extensive areas, which makes proactive response difficult (Wilhite and Glantz 1985; Mishra and Singh 2010). Hydrological drought develops when precipitation deficits propagate into reduced streamflow and manifests as a shortage of available water resources, directly affecting water supply and the operation of water resources infrastructure (Van Loon 2015). Therefore, evaluating water resources management risk under climate change requires a quantitative analysis

of the occurrence characteristics and hazard levels of hydrological drought. Drought events are generally defined on the basis of run theory and characterized by duration, severity and intensity (Yevjevich 1967), and their probabilistic risk level is evaluated through frequency analysis in terms of return periods or exceedance probabilities. Because drought is a compound phenomenon in which duration and severity are mutually dependent, bivariate drought frequency analysis accounting for this interdependence has been widely applied (Shiau 2006). Deger et al. (2023) performed univariate and copula-based bivariate drought frequency analyses of the duration and severity of drought events identified with the streamflow drought index for the Euphrates basin in Türkiye and showed that the joint return periods revealed spatial differences in drought risk within the basin. More recently, climate change scenarios have been incorporated into bivariate drought frequency analysis to assess future drought risk (Kim et al. 2019; Singh et al. 2026). Using 19 general circulation model (GCM) projections under representative concentration pathway (RCP) 8.5, Kim et al. (2019) conducted a bivariate drought frequency analysis for 109 middle-sized watersheds in South Korea and found that the projected mean duration of future droughts remained similar to that of the historical period, whereas projected drought severity increased. Using 13 GCM projections under Shared Socioeconomic Pathway 5-8.5 (SSP5-8.5), Singh et al. (2026) performed a conditional bivariate drought frequency analysis for a semi-arid basin in India and projected increases of 10-41% in drought severity and 12-35% in duration.

Such analyses presuppose specific SSP scenarios or GCM combinations. The results therefore depend strongly on the scenarios and climate models selected. In these top-down approaches, which evaluate future impacts on the basis of climate projections, uncertainty accumulates at each step of the projection chain, and a reanalysis is required whenever new scenarios or climate models are released, which makes it difficult to incorporate uncertain projections consistently into water

management decisions (Wilby and Dessai 2010). The scenario-neutral approach was proposed to overcome these limitations: instead of starting from specific climate projections, it defines an exposure space spanning the plausible range of climate variables and systematically analyzes the system response across these climate conditions (Prudhomme et al. 2010; Brown et al. 2012; Culley et al. 2016). Prudhomme et al. (2010) introduced this concept and, for the Enrick and Roding catchments in the United Kingdom, constructed catchment-specific flood response surfaces by perturbing precipitation and temperature and combined them with multi-model climate projections, showing that flood responses differed among catchments under identical climate change conditions and that the existing design allowance of a 20% increase in flood magnitude could be exceeded under some projections. Brown et al. (2012) proposed decision scaling, in which a system response function is constructed over a wide range of climate conditions, the vulnerable domain in which system performance deteriorates is identified, and climate model projections are then combined with that domain; they applied it to an urban water supply system in Massachusetts, United States, to evaluate the risk to water supply reliability under climate change. Culley et al. (2016) derived optimal operating policies over a climate exposure range for the Lake Como water resources system in Italy, defined the failure boundary beyond which the minimum performance requirement cannot be maintained by operating policies alone as the maximum operational adaptive capacity of the system, and suggested that additional infrastructure upgrades may be required under climate conditions beyond that boundary.

Existing scenario-neutral studies, however, have focused mainly on identifying the critical conditions or vulnerable domains of a system, and the system response has mostly been evaluated with a single performance indicator. In contrast, hydrological drought exhibits interdependence between duration and severity, so individual characteristics alone cannot fully describe the joint

92 occurrence probability of drought events. A probabilistic drought indicator that reflects the
93 interdependence of duration and severity therefore needs to be adopted as the scenario-neutral
94 response variable to evaluate changes in drought hazard under diverse climate conditions. Studies
95 combining such probabilistic bivariate drought frequency analysis with the scenario-neutral
96 approach, however, remain limited. This study therefore constructs scenario-neutral response
97 surfaces using the joint return period of drought duration and severity as the system response
98 variable and evaluates the probabilistic changes in hydrological drought hazard with changing
99 climate conditions over the precipitation-temperature exposure space.
100 The overall objective of this research is to establish a framework for assessing hydrological
101 drought hazard under climate change and using the resulting hazard information to determine
102 watershed-level management priorities. To address these two methodological components
103 separately, the research is presented as a two-part series. Part 1 assesses hydrological drought
104 hazard for 113 middle-sized watersheds in South Korea across a precipitation-temperature
105 exposure space using a scenario-neutral approach, whereas Part 2 applies the resulting hazard
106 information to the classification of drought management priorities.
107 As Part 1 of the series, the present study focuses on assessing hydrological drought hazard under
108 a range of climate conditions. Daily streamflow was simulated for each watershed using
109 meteorological observations for 1973-2025, and bivariate drought frequency analysis was
110 conducted to estimate the joint return period of drought duration and severity. Scenario-neutral
111 response surfaces of the design drought return period were subsequently developed across the
112 precipitation-temperature exposure space through climate stress testing. Finally, 72 climate
113 projections consisting of 4 SSPs and 18 GCMs were mapped onto the response surfaces for the

near future (NF, 2026-2060) and far future (FF, 2061-2100) to evaluate changes in hydrological drought hazard under future climate conditions.

2 Data and Methods

2.1 Study Area and Data

The study area comprises the 113 middle-sized watersheds of South Korea in East Asia (Fig. 1). South Korea lies between 33-39°N and 124-131°E with an area of about 100,472.4 km²; mean annual precipitation is approximately 1,000-1,800 mm and mean annual temperature is 11-14℃. About 70% of the annual precipitation is concentrated in the summer monsoon season from June to September, so that floods recur in summer and droughts in spring and winter, resulting in pronounced seasonal variability in water availability. In addition, about 70% of the territory is mountainous, and the five major river basins encompass diverse terrain including plains, coasts and islands, so hydrological responses and drought vulnerability differ among regions and regionally tailored water resources management is required.

For the historical period (1973-2025), daily precipitation and daily mean, maximum and minimum temperature were collected from 57 weather stations of the Korea Meteorological Administration. The stations are marked in black in Fig. 1, and the point data were spatially aggregated into watershed-averaged series using the Thiessen polygon method.

[**Fig. 1** Location of the 5 major river basins and 113 middle-sized watersheds in South Korea. Jeju, Ulleung, and Dokdo islands are excluded, and hatched watersheds indicate watersheds discussed in the manuscript]

For the future period (2026-2100), GCM projections from the Coupled Model Intercomparison Project Phase 6 under the SSP scenarios were used. All four pathways (SSP1-2.6, SSP2-4.5, SSP3-7.0 and SSP5-8.5), which differ in the degree of challenge to mitigation and adaptation and represent the low-emission, intermediate, high-challenge and high-emission scenarios, respectively, were used. 18 GCMs were used for each SSP, with station-scale daily projections downscaled and bias-corrected by the Rural Development Administration of Korea with the Simple Quantile Mapping (SQM) technique. SQM belongs to the family of empirical quantile-mapping transformations that are widely used to downscale and bias-correct climate model output to the station scale (Gudmundsson et al. 2012; Cannon et al. 2015). Information on the GCMs used for each SSP scenario is given in Table 1.

[**Table 1** Information about the GCMs used in this study]

2.2 Long-term Runoff Simulation

Because long-term continuous observed streamflow records are not available for all middle-sized watersheds in Korea, consistent nationwide hydrological drought analysis requires a consistent set of simulated streamflow. In this study, daily streamflow was simulated for each watershed with the Génie Rural à 4 paramètres Journalier (GR4J) rainfall-runoff model. GR4J is a parsimonious conceptual rainfall-runoff model that simulates daily discharge at the watershed outlet from precipitation and potential evapotranspiration inputs (Perrin et al. 2003). It has four parameters: x1 is the maximum capacity of the production store (mm), x2 is the groundwater exchange coefficient (mm d^{-1}), x3 is the one-day-ahead maximum capacity of the routing store (mm), and x4 is the time base of the unit hydrograph UH1 (d). The model structure and detailed computations are given in Perrin et al. (2003).

Daily precipitation for 1973-2025 and potential evapotranspiration estimated from the temperature data (mean, maximum and minimum) with the Hargreaves-Samani equation was used as inputs (Hargreaves and Samani 1985). Daily inflow records of 21 multipurpose dam catchments in Korea were used for parameter calibration. To remove the influence of the initial storage states, the first year (1973) was treated as a warm-up period and excluded from the performance evaluation, so that the calibration and analysis period is 1974-2025. The modified Kling-Gupta efficiency (KGE′) was used as the objective function (Kling et al. 2012). KGE′ is a variant of the Kling-Gupta efficiency of Gupta et al. (2009) in which the variability term is expressed as the ratio of the coefficients of variation rather than the ratio of the standard deviations. KGE′ evaluates the correlation, bias and variability components separately and is defined in Eq. (1); values closer to 1.0 indicate better simulation performance.

$$KGE' = 1 - \sqrt{(r-1)^2 + (\beta-1)^2 + (\gamma-1)^2} \quad (1)$$

where r is the Pearson correlation coefficient between the observed and simulated flows, β is the ratio of the simulated to observed mean flow, and γ is the ratio of the simulated to observed coefficients of variation. The parameter search ranges were restricted to the 80% confidence intervals given by Perrin et al. (2003) (x1: 100-1,200 mm; x2: −5 to 3 mm d^{-1}; x3: 20-300 mm; x4: 1.1-2.9 d) to ensure the physical plausibility of the optimum. The GR4J parameters were optimized with the differential evolution algorithm (Storn and Price 1997).

Year-wise leave-one-year-out cross-validation (LOOCV) was performed for the 21 multipurpose dam catchments, and the watersheds with validation KGE′ of 0.7 or higher were selected as the final calibration watersheds. For the ungauged watersheds, the parameters were regionalized. Parameter transfer based on spatial proximity or physical similarity has been reported to outperform regression-based methods for ungauged basins (Oudin et al. 2008; Zhang and Chiew

2009). The donor search was therefore restricted to the calibrated watersheds within the same major river basin as the target watershed, and where no calibrated watershed exists in the same major river basin, all calibrated watersheds were taken as candidates. Where two or more candidates exist, three attributes, such as mean annual precipitation, the aridity index (the ratio of annual potential evapotranspiration to annual precipitation) and watershed area, were standardized by the mean and standard deviation of the calibration set, and the parameters of the calibrated watershed with the smallest Euclidean distance in the standardized space were transferred (Parajka et al. 2005). The validity of the parameter transfer was evaluated by LOOCV, in which each donor watershed was treated as ungauged and the parameters of the substitute donor selected by the same rule were applied.

2.3 Definition of Drought Events

Hydrological drought events were extracted with the threshold level method (Yevjevich 1967). For each day τ, the threshold discharge $Q_0(\tau)$ was computed as the 20% non-exceedance quantile of all discharge values within a ±15-day window centered on τ pooled over the entire record (Q_{80}) and was smoothed with a 30-day moving average (Hisdal et al. 2004; Van Loon 2015). A period during which the discharge continuously falls below the threshold was defined as one drought event; the duration is the number of consecutive days below the threshold, and the severity is the accumulated difference between the threshold and the actual discharge over that period.

Adjacent drought events were pooled with the inter-event criterion (IC) (Tallaksen et al. 1997; Fleig et al. 2006). Two successive events were merged when the inter-event time t_i is at most the critical interval t_c and the ratio of the excess volume above the threshold during the interval v_i to the severity of the preceding event s_i is at most the threshold ρ_c. The pooling condition is defined

in Eq. (2), and two successive events are merged when $M_i = 1$. When two events are merged, the duration of the pooled event is the sum of the two durations and the intervening interval. Its severity is the sum of severities of two events subtracting the excess volume accumulated during the inter-event interval.

$$M_i = 1\left[t_i \le t_c \quad \text{and} \quad \frac{v_i}{s_i} \le \rho_c\right] \tag{2}$$

where M_i is the pooling indicator for the ith pair of successive drought events, t_i is the inter-event time, t_c is the critical inter-event time, v_i is the excess volume above the threshold during the inter-event interval, s_i is the severity of the preceding drought event, and ρ_c is the critical pooling threshold. The critical interval was set to $t_c = 5$ days (Tallaksen et al. 1997; Fleig et al. 2006). ρ_c was determined for each watershed as the upper candidate ρ at which the change in the final number of drought events $N(\rho)$, computed while varying the candidate value from 0 to 1 in increments of 0.05, is largest.

$$\rho_c = \rho_{k+1}, \qquad k = \arg\max_k |N(\rho_{k+1}) - N(\rho_k)|, \qquad \rho_k \in \{0, 0.05, \ldots, 1\} \tag{3}$$

where ρ_k is the kth candidate value of the pooling threshold, $N(\rho_k)$ is the final number of drought events obtained using ρ_k, and k is the index that maximizes the absolute change in the number of drought events between adjacent candidate thresholds. If the event count was identical for all candidate values of ρ, $\rho_c = 0.5$ was applied. Events with a duration of 5 days or less were excluded from the analysis.

2.4 Bivariate Drought Frequency Analysis

To estimate the joint return period of drought duration and severity, copula-based bivariate frequency analysis was applied (Salvadori and De Michele 2004; Shiau 2006). Following the

225 theorem of Sklar (1959), the joint distribution $H(d, s)$ of the two variables is expressed as the
226 combination of the marginal distributions and a copula function.

$$H(d,s) = C\big(F_D(d), F_S(s)\big) = C(u,v) \tag{4}$$

227 where $H(d, s)$ is the joint cumulative distribution function of drought duration and severity, $F_D(d)$
228 and $F_S(s)$ are their marginal cumulative distribution functions, $C(\cdot)$ is the copula function, and
229 $u = F_D(d)$ and $v = F_S(s)$ are the corresponding non-exceedance probabilities. The marginal
230 distributions of duration and severity were fitted by maximum likelihood among 8 candidates: the
231 exponential, normal, gamma, lognormal, Weibull, generalized extreme value (GEV), generalized
232 Pareto (GPD) and Gumbel distributions. For each watershed, the distribution with the largest p-
233 value in the Kolmogorov-Smirnov (KS) test was selected as the best marginal distribution (Coles
234 2001). The Clayton, Frank and Gumbel copulas of the Archimedean family were considered as
235 candidates for the dependence structure. The parameter of each copula was estimated by maximum
236 likelihood, and the copula with the largest log-likelihood was selected as the best model for each
237 watershed (Genest and Favre 2007). For a bivariate drought event, two types of joint exceedance
238 conditions can be considered: the OR and AND conditions (Salvadori and De Michele 2004; Shiau
239 2006). The OR condition represents an event in which either drought duration or severity exceeds
240 a specified level, whereas the AND condition represents an event in which both duration and
241 severity exceed their specified levels simultaneously. Because this study focuses on drought events
242 characterized by both long duration and high severity, the AND condition was adopted to quantify
243 the joint exceedance probability of two drought characteristics. The joint exceedance probability
244 under the AND condition was computed as follows.

$$p_i = P(D \geq d_i, S \geq s_i) = 1 - u_i - v_i + C(u_i, v_i) \tag{5}$$

where p_i is the joint exceedance probability of the ith drought event, D and S denote drought duration and severity, respectively, d_i and s_i are the observed duration and severity of event i, and $u_i = F_D(d_i)$ and $v_i = F_S(s_i)$. In this study, the observed event with the smallest joint exceedance probability p_i was defined as the design drought, and the corresponding joint exceedance probability was set to p^*. The joint return period of the design drought T_{DS} was computed from the mean inter-event arrival time E(L) and p^* as follows (Shiau 2006).

$$T_{DS} = \frac{E(L)}{p^*} \tag{6}$$

where E(L) is the mean inter-arrival time of drought events (year).

2.5 Scenario-neutral Response Surfaces

Hydrological sensitivity to climate change was evaluated with the scenario-neutral approach (Prudhomme et al. 2010; Brown et al. 2012). Instead of using scenario projections directly as inputs, the response of the design drought return period was first constructed over an exposure space in which precipitation and temperature changes were imposed systematically, and the climate projections were then overlaid on the response surface.

2.5.1 Generation of the Climate Stress Time Series

Climate stress time series under precipitation and temperature changes were generated with a multi-site stochastic weather generator (Richardson 1981; Wilks 1998; Steinschneider and Brown 2013). Daily precipitation occurrence was simulated with a monthly first-order two-state Markov chain, and wet-day precipitation amounts were generated from the inverse of the monthly, station-specific empirical cumulative distribution function. The precipitation change was applied using the following change-factor approach.

$$P_t^* = P_t\left(1 + \frac{\Delta P}{100}\right) \quad (7)$$

where P_t and P_t^* are the baseline and perturbed daily precipitation on day t, respectively, and ΔP is the annual precipitation change (%). Daily temperature was generated with the daily climatological mean and residuals simulated using a first-order autoregressive process to preserve temporal persistence (Richardson 1981), and the temperature change was applied as follows.

$$T_t^* = T_t + \Delta T \quad (8)$$

where T_t and T_t^* are the baseline and perturbed daily temperature, respectively, and ΔT is the temperature change (℃). Spatial dependence among stations was reproduced with the normal-score transformation and a Gaussian copula.

The exposure space consisted of combinations of ΔP and ΔT. Its range was set to cover the range of changes of the four SSPs, 18 GCM projections used in this study, with ΔP from −20 to +80% (5% intervals, 21 levels) and ΔT from 0 to +11 ℃ (1℃ intervals, 12 levels), giving 252 climate conditions in total. For each climate condition a 53-year climate series was generated, and the runoff simulation, drought event extraction and bivariate frequency analysis of Sections 2.2-2.4 were applied to compute the joint return period of the design drought T_{DS}. The marginal and copula families, the design drought and the threshold discharge were fixed at the baseline selections, and only the distribution parameters were re-estimated for each climate condition.

2.5.2 Construction of the Response Surface and Definition of the Baseline

The watershed-specific climate response surface was constructed by smoothing the T_{DS} values computed at the 252 climate conditions over the $\Delta P - \Delta T$ plane with multivariate locally weighted regression (LOESS; Cleveland 1979; Cleveland and Devlin 1988).

$$\hat{T}_{DS} = f(\Delta P, \Delta T) \quad (9)$$

where $\hat{T}_{DS}$ is the design drought return period estimated from the response surface and $f(\cdot)$ is the LOESS response surface after back-transformation to the return-period scale. The adequacy of the response surfaces was evaluated with the coefficient of determination (R^2) and the root mean square error of the log-space residuals at the 252 nodes.

A nonparametric smoother was adopted so that no functional form is imposed on the stress-response relationship. The two perturbation axes were standardized by their mean and standard deviation, and at each query point a locally linear fit with tricube weights was obtained over the k nearest nodes, where k is the span fraction of the 252 nodes (span 0.5) subject to a minimum of 12 nodes.

The fit near the baseline was additionally diagnosed with the sign disagreement rate, defined as the proportion of nodes at which the sign of the change relative to the baseline value differs between the fitted surface and the directly simulated node value before smoothing.

Three baseline concepts are defined in this study. First, the baseline point is the condition $(\Delta P, \Delta T) = (0, 0)$, in which no change is imposed on precipitation or temperature. It corresponds to the observed climate of 1974-2025 to which the weather generator was calibrated. Second, the baseline return period is the return period estimated by the response surface at the baseline point, defined as follows.

$$T_{DS}^{0} = f(0, 0) \quad (10)$$

where T_{DS}^{0} is the baseline return period estimated from the response surface at $(\Delta P, \Delta T) = (0, 0)$. Third, the baseline isoline is the contour of the response surface satisfying $\hat{T}_{DS} = T_{DS}^{0}$; it separates the region in which the return period falls below the baseline from the region in which it rises above.

The baseline return period T_{DS}^{0} is distinct from T_{DS} computed directly from the simulated streamflow in Section 2.4: the former is a value on the smoothed surface, whereas the latter is estimated directly from the individual drought events. All change ratios reported for the climate projections are taken relative to the baseline value of the same fitted surface, so that the reference and the compared value originate from the same generated-climate data set and the sampling difference between the generated and the observed series does not enter the change ratio. The agreement between the two values was evaluated with the rank correlation coefficient.

2.5.3 Local Sensitivities and the Compensating Precipitation Ratio

Although the response surface describes the overall response of the design drought return period across the precipitation-temperature exposure space, it does not directly quantify the magnitude of the response to each climate variable near the baseline condition. Local sensitivities were therefore calculated to compare the responses to changes in precipitation and temperature among watersheds. Because precipitation increase and warming generally affect the return period in opposite directions, the compensating precipitation ratio was defined to quantify the precipitation increase required to offset the effect of warming. The local sensitivities near the baseline point were computed as in Eq. (11).

$$S_P = \frac{\log f(h_P,0) - \log f(-h_P,0)}{2h_P}, \quad S_T = \frac{\log f(0,h_T) - \log f(0,-h_T)}{2h_T} \tag{11}$$

where $h_P = 5\%$ and $h_T = 1$ ℃ are the finite-difference step sizes for precipitation and temperature, respectively, and S_P and S_T are the local sensitivities of $\log T_{DS}$ to precipitation and temperature changes, respectively. $S_P > 0$ indicates that an increase in precipitation makes the design drought rarer, and $S_T < 0$ that warming makes a drought of the same magnitude more frequent. Absolute values of the two sensitivities were used when comparing major river basins.

The ratio of the two sensitivities was then defined as the compensating precipitation ratio.

$$\pi_c = -\frac{S_T}{S_P} \tag{12}$$

where π_c is the compensating precipitation ratio (%/°C), defined as the increase in annual precipitation required to offset the effect of 1 °C of warming on the design drought return period. The larger the value, the greater the increase in precipitation required for a watershed to offset the effects of warming.

The direction of the response over the whole exposure space was evaluated with the Spearman rank correlation of $\Delta P - \hat{T}_{DS}$ and $\Delta T - \hat{T}_{DS}$ over 252 nodes.

2.5.4 Deterioration Area Fraction

The size of the region in which the return period falls below the baseline over the whole exposure space was defined as the deterioration area fraction.

$$F_{det} = \frac{1}{N_g}\sum_{i=1}^{N_g} \mathbb{1}\left[\hat{T}_{DS,i} < T_{DS}^{0}\right] \tag{13}$$

where F_{det} is the deterioration area fraction, $N_g = 252$ is the total number of evaluation nodes, i denotes the node index, $\mathbb{1}(\cdot)$ is the indicator function that equals 1 when $\hat{T}_{DS,i} < T_{DS}^{0}$ and 0 otherwise, and $\hat{T}_{DS,i}$ is the return period estimated from the response surface at node i. F_{det} ranges from 0 to 1. A larger value indicates that the deteriorating region occupies a larger proportion of the examined exposure space. It was interpreted as an index for comparing watershed climate-response characteristics independently of where the projections of a particular scenario or climate model lie.

2.5.5 Projection of the Climate Scenarios and Change Metrics

The future climate change impact was assessed by projecting the NF and FF precipitation and temperature changes $(\Delta P_g, \Delta T_g)$ of the 18 GCMs under the four SSP scenarios onto the response surfaces, and the design drought return period under each climate projection was computed as follows.

$$\hat{T}_{DS,g} = f(\Delta P_g, \Delta T_g) \tag{14}$$

where $\hat{T}_{DS,g}$ is the design drought return period estimated for climate projection g, and ΔP_g and ΔT_g are the precipitation and temperature changes associated with projection g, respectively. Projection g is defined by the combination of SSP s, period t, and GCM k. Projection points outside the exposure space were clipped to its boundary. For each SSP-period combination the median of the 18 GCM projections was compared with the baseline return period to obtain the change ratio.

$$\delta_{s,t} = \frac{\underset{g \in G_{s,t}}{\text{median}}\, \hat{T}_{DS,g} - T_{DS}^0}{T_{DS}^0} \times 100 \tag{15}$$

where $\delta_{s,t}$ is the percentage change in the ensemble-median design drought return period for SSP s and period t relative to the baseline, and $G_{s,t}$ is the set of $n = 18$ GCM projections for the corresponding SSP-period combination. Separately from the central tendency of the ensemble, the proportion of projections with a return period below the baseline was also computed.

$$q_{s,t} = \frac{1}{n} \sum_{g \in G_{s,t}} \mathbb{1}\left[\hat{T}_{DS,g} < T_{DS}^0\right] \tag{16}$$

where $q_{s,t}$ is the proportion of GCM projections for SSP s and period t in which the projected design drought return period is below the baseline return period. A watershed with $\delta_{s,t} > 0$ and $q_{s,t} > 0$ is one in which the design drought becomes rarer at the ensemble median while becoming more frequent under some projections, so that the unfavourable projections are not revealed by the

central tendency alone. Differences in climate sensitivity among the major river basins were analyzed with the Kruskal-Wallis test.

3 Results

3.1 Long-term Runoff Simulation Results

After calibration against the daily inflow records of the 21 multipurpose dam catchments and year-wise LOOCV, seven watersheds met the validation criterion of KGE′ ≥ 0.7 (Table 2). The 7 watersheds that met the validation criterion were used as donors, and for the remaining 106 middle-sized watersheds the GR4J parameters were estimated by regionalization based on the major river basin constraint and physical similarity. Daily streamflow for 1974-2025 was thereby simulated for all 113 middle-sized watersheds and used as input to the hydrological drought analysis.

[Table 2 Parameters and performance of the GR4J model for the 7 calibrated watersheds (NSE, Nash–Sutcliffe efficiency; KGE′, modified Kling–Gupta efficiency; cal., calibration; val., validation)**]**

3.2 Estimation of the Design Drought Return Period

Drought events were identified by applying the variable threshold level method (Q_{80}) and the IC method to the simulated daily streamflow for 1974-2025. The GEV distribution was selected as the best marginal distribution of drought duration in 101 of the 113 watersheds and the lognormal distribution in 12 watersheds (Table 3). The median p-value of the KS test was 0.30, although in three watersheds all candidate distributions were rejected at the 0.05 significance level and the distribution with the best goodness of fit was applied. For drought severity, the lognormal distribution was selected most frequently, in 59 watersheds, followed by the GEV in 24, the GPD

391 in 23 and the Weibull in seven watersheds. The severity marginals satisfied the KS test at the 0.05
392 level in all watersheds. For the dependence structure between duration and severity, the Gumbel
393 copula was selected from 104 watersheds and the Clayton copula in nine watersheds.
394
395 [**Table 3** Selected marginal distributions and copula families of drought duration and severity by
396 major river basin (GEV, generalized extreme value; LN, lognormal; GPD, generalized Pareto;
397 WBL, Weibull)]
398
399 The median duration of the design droughts was 147 days, with an interquartile range of 87-194
400 days and a full range of 35-311 days. The median severity of the design droughts was about 19.2
401 million m³, with an interquartile range of about 9.1-31.7 million m³ and a full range of about 0.51-
402 79.7 million m³, showing large differences among watersheds.
403 T_{DS} had a national median of 29.8 years, with an interquartile range of 19.5-45.2 years. By return
404 period class, 31 watersheds were below 20 years, 57 between 20 and 50 years, 11 between 50 and
405 100 years and 14 above 100 years. The medians by major river basin were 33.5 years for the
406 Nakdong River basin, 32.8 for the Han River basin, 31.1 for the Seomjin River basin, 23.4 for the
407 Yeongsan River basin and 21.5 for the Geum River basin. The comparatively short return periods
408 of the Geum River basin and Yeongsan River basin indicate that their design droughts can recur
409 relatively frequently. By contrast, 11 of the 14 watersheds exceeding 100 years belong to the Han
410 River basin, where the joint exceedance probability of the design event is very small and the return
411 period is estimated in the extrapolation range of the fitted distributions.
412
413 **3.3 Response Surfaces of the Return Period**

414 The watershed-specific goodness of fit (R^2) of the response surfaces ranged from 0.568 to 0.932,
415 with a median of 0.879. R^2 was 0.8 or higher in 103 of the 113 watersheds (91.2%), indicating
416 overall good agreement. The T_{DS} estimated at the baseline point of the response surface ranged
417 from 10.8 to 198.9 years with a median of 46.5 years across watersheds. The median of the
418 baseline-period T_{DS} computed directly from the baseline simulated streamflow was 29.8 years, and
419 the rank correlation between the two values was 0.834.
420 R^2 of the response surface was below 0.8 in ten watersheds, including five in the Han River basin,
421 four in the Nakdong River basin, and one in the Seomjin River basin. These watersheds included
422 cases with long baseline return periods lying in the extrapolation range, such as the Lower Imjin
423 River watershed (#1023) and Wangpicheon watershed (#2401). The response surfaces showed that
424 in every watershed the design drought return period decreases with decreasing precipitation and
425 rising temperature (Fig. 2). The rank correlation of $\log T_{DS}$ with the precipitation change had a
426 median of 0.848 across watersheds and a minimum of 0.509. The rank correlation with the
427 temperature change had a median of −0.240 and a maximum of −0.123, negative in every
428 watershed. The representative watersheds in Figs. 2 and four watersheds were selected as those
429 with the largest deterioration area fraction within each major river basin.
430
431 [**Fig. 2** Scenario-neutral response surfaces of the design drought return period (T_{DS}) for the
432 representative watersheds selected from each major river basin]
433
434 The median local sensitivities across watersheds computed at the baseline point $(\Delta P, \Delta T) = (0,0)$
435 indicated that $\log T_{DS}$ increased by 0.041 per 1% increase in precipitation and decreased by 0.103
436 per 1°C of warming. Because these are changes in the log return period, they correspond to an

increase of about 4.2% in the return period per 1% increase in precipitation and a decrease of about 9.8% per 1℃ of warming.

The baseline-point sensitivities differed among major river basins. The absolute values of both the precipitation and the temperature sensitivity were largest in the Yeongsan River basin and smallest in the Han River basin, and the differences among major river basins were statistically significant (Kruskal-Wallis, $p < 0.001$ and $p = 0.002$, respectively). The compensating precipitation ratio, defined by the slope of the baseline isoline, had a national median of a 2.64% increase in precipitation per 1℃ of warming, with no significant difference among major river basins ($p = 0.366$) (Fig. 3).

[Fig. 3 Distributions of the response-surface sensitivities by major river basin: (a) precipitation sensitivity and (b) temperature sensitivity**]**

3.4 Climate Change Impact Assessment Based on the Response Surfaces

When the SSP-wise GCM projections were overlaid on the response surfaces, the range of change in the design drought return period differed by SSP and analysis period (Fig. 4). Based on the GCM ensemble median for each watershed, the national median change in T_{DS} was +16.6% (SSP3-7.0) to +33.3% (SSP5-8.5) in the NF and +33.5% (SSP3-7.0) to +55.3% (SSP5-8.5) in the FF, an increase relative to the baseline for all SSP-period combinations. Among the SSPs, the increase in return period was smallest under SSP3-7.0 and largest under SSP5-8.5.

[**Fig. 4** SSP–GCM projections for the NF and FF overlaid on the scenario-neutral response surfaces for the representative watersheds selected from each major river basin]

At the level of individual GCM projection points, the proportion of points at which the return period decreased relative to the baseline T_{DS} was 13.5-31.3% across the SSP-period combinations: 19.6-31.3% in the NF and 13.5-24.4% in the FF. The proportion of decreasing points was highest in the NF of SSP3-7.0 (31.3%) and lowest in the FF of SSP5-8.5 (13.5%).

The spread of the GCM projections widened toward the FF. The range of the GCM-wise national median T_{DS} was 30.0-110.6 years in the NF and 34.7-162.8 years in the FF, and the width of the range widened from 59.2-73.2 years to 85.5-128.1 years for every SSP. Within the same SSP, moreover, the return period increased for some GCMs and decreased for others, with the widest spread in the FF of SSP5-8.5. The possibility of decreasing return periods in the lower tail of the GCM projections therefore needs to be evaluated separately from the central tendency.

4 Discussion

In the climate change impact assessment, the GCM ensemble median indicated an increase in the design drought return period relative to the baseline for all SSP-period combinations, which means a lower probability of occurrence of a drought event of the same magnitude. At the level of individual GCM projection points, however, the return period decreased at 13.5-31.3% of the points, with change ratios of −35.2 to +187.7%, indicating that the central tendency of the ensemble alone may not adequately reflect some unfavorable projections. Previous studies have also shown that the direction and magnitude of future drought changes can vary substantially among climate projections and regions. Kim et al. (2019), based on 19 RCP8.5 climate projections for 109 middle-sized watersheds in South Korea, reported that future drought duration remained generally similar to that of the control period, whereas drought severity increased in most projections, with considerable differences in drought risk among GCMs and river basins.

Madadgar and Moradkhani (2013), in contrast, projected decreases in drought duration and severity in the Upper Klamath River Basin, with all 5 GCM projections producing longer drought return periods than those of the historical period, although substantial GCM-related uncertainty remained. At a broader spatial scale, Forzieri et al. (2014) found that future streamflow droughts became more severe and persistent across much of southern Europe but decreased in northern and northeastern Europe, with greater disagreement among model projections in transition regions. Although these studies differ in drought definition, spatial scale, and climate forcing, their results demonstrate that future drought hazard may vary in both magnitude and direction depending on the climate projection and regional hydrological response.

The present results provide a hydrological interpretation of these projection-dependent differences through the precipitation-temperature response surfaces. In every watershed, the design drought return period increased with increasing precipitation and decreased with rising temperature, and the compensating precipitation ratio had a national median of 2.64% per 1℃ of warming. At the ensemble median, the precipitation increase per 1℃ of warming exceeded the compensating precipitation ratio for every SSP-period combination, resulting in an increase in the return period. In contrast, the return period decreased under some individual GCM projections for which the precipitation increase was insufficient to offset the effect of warming.

Compared with previous scenario-neutral applications, the methodological contribution of the present study lies primarily in the response variable used to characterize climate sensitivity. Previous studies have evaluated climate responses using measures such as flood magnitude, water-supply reliability, or operational performance (Prudhomme et al. 2010; Brown et al. 2012; Culley et al. 2016). In contrast, the present study uses the joint return period of drought duration and severity as the response variable, allowing changes in the occurrence probability of a bivariate

506 hydrological drought event to be evaluated directly over the precipitation-temperature exposure
507 space. Furthermore, applying the same framework to 113 middle-sized watersheds provides a
508 consistent basis for comparing watershed-specific climate sensitivity and for identifying the
509 climate conditions under which drought hazard increases or decreases.
510 This study has several limitations. First, long-term observed streamflow is not available for all 113
511 middle-sized watersheds, and the GR4J parameters from seven donor watersheds that met the
512 validation criteria were therefore regionalized to the remaining watersheds. Considering the
513 regionalization uncertainty, the results should be interpreted with a focus on the relative
514 differences among watersheds rather than on the absolute values of individual watersheds.
515 Second, the direction of change estimated from the response surface showed relatively high
516 uncertainty near the baseline. Because the disagreement in the direction of change between the
517 direct simulations and the response surface was large at points where the magnitude of change was
518 small, the results in the region adjacent to the baseline should be interpreted with caution.
519 Third, the climate stress test compares the responses to changes in climate conditions while
520 keeping the drought definition and the probabilistic structure set for the baseline condition, so the
521 threshold discharge, the marginal distributions, the copula family and the design drought selected
522 in the baseline period were fixed and only the distribution parameters were re-estimated for each
523 climate condition. Changes in the distributional form of drought events or in the dependence
524 structure between duration and severity under long-term climate change are therefore not reflected,
525 and this assumption needs to be considered when interpreting the results.
526

527 **5 Conclusion**

This first paper of a two-part series quantified the hydrological drought hazard of the 113 middle-sized watersheds of South Korea within a scenario-neutral framework. Daily streamflow for 1974-2025 was simulated with the GR4J model, drought events were defined with the variable threshold level method and inter-event pooling, and the design drought return period was estimated by copula-based bivariate frequency analysis of duration and severity. Scenario-neutral response surfaces of the return period were constructed from 252 precipitation-temperature perturbation combinations, with watershed-specific R^2 values of 0.568-0.932. When the projections of the 18 GCMs under the four SSPs were overlaid on the response surfaces, the design drought return period increased relative to the baseline for all SSP-period combinations at the GCM ensemble median, whereas the return period decreased at 13.5-31.3% of the individual projection points and the spread of the projections widened toward the FF.

The baseline design droughts, the response surfaces and the SSP-GCM projection overlays constructed here provide a transferable basis for watershed-level drought hazard assessment. By using the joint return period of drought duration and severity as the system response, the framework extends scenario-neutral climate stress testing to probabilistic bivariate hydrological drought assessment. The contrasting effects of precipitation change and warming, together with the differences between the ensemble-median and individual GCM responses, also indicate that hydrological drought hazard cannot be fully characterized by the central tendency of climate projections alone. Because the response surfaces describe hydrological responses over the broader precipitation-temperature exposure space, newly available climate projections can be evaluated within the same framework without repeating the hydrological simulation chain. These hazard products provide direct inputs to the risk-informed drought management assessment developed in

Part 2, in which watersheds exposed to greater hazard under adverse projections are distinguished from those that remain relatively stable.

Statements and Declarations

Funding

This work was supported by the Korea Environmental Industry & Technology Institute (KEITI) through the Climate Resilient R&D Project for Water-Related Disaster Management, funded by the Korea Ministry of Climate, Energy and Environment (MCEE) (RS-2022-KE002032).

Competing Interests

The authors have no competing interests to declare that are relevant to the content of this article.

Data Availability

Data can be provided upon request.

Author Contributions

Conceptualization, methodology, formal analysis and writing — original draft: Jiyoung Kim; supervision and writing — review and editing: Tae-Woong Kim. All authors read and approved of the final manuscript.

References

Brown C, Ghile Y, Laverty M, Li K (2012) Decision scaling: linking bottom-up vulnerability analysis with climate projections in the water sector. Water Resour Res 48(9):W09537. https://doi.org/10.1029/2011WR011212

Cannon AJ, Sobie SR, Murdock TQ (2015) Bias correction of GCM precipitation by quantile mapping: how well do methods preserve changes in quantiles and extremes? J Clim 28(17):6938-6959. https://doi.org/10.1175/JCLI-D-14-00754.1

Cleveland WS (1979) Robust locally weighted regression and smoothing scatterplots. J Am Stat Assoc 74(368):829-836. https://doi.org/10.1080/01621459.1979.10481038

Cleveland WS, Devlin SJ (1988) Locally weighted regression: an approach to regression analysis by local fitting. J Am Stat Assoc 83(403):596-610. https://doi.org/10.1080/01621459.1988.10478639

Coles S (2001) An introduction to statistical modeling of extreme values. Springer, London. https://doi.org/10.1007/978-1-4471-3675-0

Culley S, Noble S, Yates A, Timbs M, Westra S, Maier HR, Giuliani M, Castelletti A (2016) A bottom-up approach to identifying the maximum operational adaptive capacity of water resource systems to a changing climate. Water Resour Res 52(9):6751-6768. https://doi.org/10.1002/2015WR018253

Deger IH, Esıt M, Yuce MI (2023) Univariate and bivariate hydrological drought frequency analysis by copula functions. Water Resour Manage 37(12):4881-4907. https://doi.org/10.1007/s11269-023-03586-x

Ficklin DL, Null SE, Abatzoglou JT, Novick KA, Myers DT (2022) Hydrological intensification will increase the complexity of water resource management. Earth's Future 10(3):e2021EF002487. https://doi.org/10.1029/2021EF002487

Fleig AK, Tallaksen LM, Hisdal H, Demuth S (2006) A global evaluation of streamflow drought characteristics. Hydrol Earth Syst Sci 10(4):535-552. https://doi.org/10.5194/hess-10-535-2006

Forzieri G, Feyen L, Rojas R, Flörke M, Wimmer F, Bianchi A (2014) Ensemble projections of future streamflow droughts in Europe. Hydrol Earth Syst Sci 18(1):85-108. https://doi.org/10.5194/hess-18-85-2014

Genest C, Favre A-C (2007) Everything you always wanted to know about copula modeling but were afraid to ask. J Hydrol Eng 12(4):347-368. https://doi.org/10.1061/(ASCE)1084-0699(2007)12:4(347)

Gudmundsson L, Bremnes JB, Haugen JE, Engen-Skaugen T (2012) Technical note: downscaling RCM precipitation to the station scale using statistical transformations - a comparison of methods. Hydrol Earth Syst Sci 16(9):3383-3390. https://doi.org/10.5194/hess-16-3383-2012

Gupta HV, Kling H, Yilmaz KK, Martinez GF (2009) Decomposition of the mean squared error and NSE performance criteria: implications for improving hydrological modelling. J Hydrol 377(1-2):80-91. https://doi.org/10.1016/j.jhydrol.2009.08.003

Hargreaves GH, Samani ZA (1985) Reference crop evapotranspiration from temperature. Appl Eng Agric 1(2):96-99. https://doi.org/10.13031/2013.26773

Hisdal H, Tallaksen LM, Clausen B, Peters E, Gustard A (2004) Hydrological drought characteristics. In: Tallaksen LM, van Lanen HAJ (eds) Hydrological drought: processes and estimation methods for streamflow and groundwater. Developments in Water Science 48. Elsevier, Amsterdam, pp 139-198

IPCC (2023) Climate Change 2023: Synthesis Report. Contribution of Working Groups I, II and III to the Sixth Assessment Report of the Intergovernmental Panel on Climate Change [Core Writing Team, Lee H, Romero J (eds)]. IPCC, Geneva, Switzerland. https://doi.org/10.59327/IPCC/AR6-9789291691647

Kim JE, Yoo J, Chung GH, Kim T-W (2019) Hydrologic risk assessment of future extreme drought in South Korea using bivariate frequency analysis. Water 11(10):2052. https://doi.org/10.3390/w11102052

Kling H, Fuchs M, Paulin M (2012) Runoff conditions in the upper Danube basin under an ensemble of climate change scenarios. J Hydrol 424-425:264-277. https://doi.org/10.1016/j.jhydrol.2012.01.011

Konapala G, Mishra AK, Wada Y, Mann ME (2020) Climate change will affect global water availability through compounding changes in seasonal precipitation and evaporation. Nat Commun 11(1):3044. https://doi.org/10.1038/s41467-020-16757-w

Madadgar S, Moradkhani H (2013) Drought analysis under climate change using copula. J Hydrol Eng 18(7):746-759. https://doi.org/10.1061/(ASCE)HE.1943-5584.0000532

Mishra AK, Singh VP (2010) A review of drought concepts. J Hydrol 391(1-2):202-216. https://doi.org/10.1016/j.jhydrol.2010.07.012

Oudin L, Andréassian V, Perrin C, Michel C, Le Moine N (2008) Spatial proximity, physical similarity, regression and ungaged catchments: a comparison of regionalization approaches based on 913 French catchments. Water Resour Res 44(3):W03413. https://doi.org/10.1029/2007WR006240

Parajka J, Merz R, Blöschl G (2005) A comparison of regionalisation methods for catchment model parameters. Hydrol Earth Syst Sci 9(3):157-171. https://doi.org/10.5194/hess-9-157-2005

Perrin C, Michel C, Andréassian V (2003) Improvement of a parsimonious model for streamflow simulation. J Hydrol 279(1-4):275-289. https://doi.org/10.1016/S0022-1694(03)00225-7

Prudhomme C, Wilby RL, Crooks S, Kay AL, Reynard NS (2010) Scenario-neutral approach to climate change impact studies: application to flood risk. J Hydrol 390(3-4):198-209. https://doi.org/10.1016/j.jhydrol.2010.06.043

Richardson CW (1981) Stochastic simulation of daily precipitation, temperature, and solar radiation. Water Resour Res 17(1):182-190. https://doi.org/10.1029/WR017i001p00182

Salvadori G, De Michele C (2004) Frequency analysis via copulas: theoretical aspects and applications to hydrological events. Water Resour Res 40(12):W12511. https://doi.org/10.1029/2004WR003133

Shiau JT (2006) Fitting drought duration and severity with two-dimensional copulas. Water Resour Manage 20(5):795-815. https://doi.org/10.1007/s11269-005-9008-9

Singh HV, Joshi N, Suryavanshi S (2026) Evaluating hydrological drought characteristics in a semi-arid river basin using the conditional copula approach under the changing climate. J Earth Syst Sci 135(2):56. https://doi.org/10.1007/s12040-026-02757-9

Sklar A (1959) Fonctions de répartition à n dimensions et leurs marges. Publications de l'Institut de Statistique de l'Université de Paris 8:229-231

Steinschneider S, Brown C (2013) A semiparametric multivariate, multisite weather generator with low-frequency variability for use in climate risk assessments. Water Resour Res 49(11):7205-7220. https://doi.org/10.1002/wrcr.20528

Storn R, Price K (1997) Differential evolution - a simple and efficient heuristic for global optimization over continuous spaces. J Glob Optim 11(4):341-359. https://doi.org/10.1023/A:1008202821328

660 Tallaksen LM, Madsen H, Clausen B (1997) On the definition and modelling of streamflow
661 drought duration and deficit volume. Hydrol Sci J 42(1):15-33.
662 https://doi.org/10.1080/02626669709492003
663 Van Loon AF (2015) Hydrological drought explained. WIREs Water 2(4):359-392.
664 https://doi.org/10.1002/wat2.1085
665 Wilby RL, Dessai S (2010) Robust adaptation to climate change. Weather 65(7):180-185.
666 https://doi.org/10.1002/wea.543
667 Wilhite DA, Glantz MH (1985) Understanding: the drought phenomenon: the role of definitions.
668 Water Int 10(3):111-120. https://doi.org/10.1080/02508068508686328
669 Wilks DS (1998) Multisite generalization of a daily stochastic precipitation generation model. J
670 Hydrol 210(1-4):178-191. https://doi.org/10.1016/S0022-1694(98)00186-3
671 Yevjevich VM (1967) An objective approach to definitions and investigations of continental
672 hydrologic droughts. Hydrology Paper No. 23, Colorado State University, Fort Collins,
673 Colorado
674 Zhang Y, Chiew FHS (2009) Relative merits of different methods for runoff predictions in
675 ungauged catchments. Water Resour Res 45(7):W07412.
676 https://doi.org/10.1029/2008WR007504

Tables

Table 1 Information about the GCMs used in this study

No	Model	Institution	Atmospheric resolution (Lon × Lat)
1	GFDL-ESM4	Geophysical Fluid Dynamics Laboratory (USA)	360×180
2	MRI-ESM2-0	Meteorological Research Institute (Japan)	320×160
3	CNRM-CM6-1	Centre National de Recherches Meteorologiques (France)	24572 grids distributed over 128 latitude circles
4	CNRM-ESM2-1		
5	IPSL-CM6A-LR	Institute Pierre-Simon Laplace (France)	144×143
6	MPI-ESM1-2-HR	Max Planck Institute for Meteorology (Germany)	384×192
7	MPI-ESM1-2-LR		192×96
8	UKESM1-0-LL	Met Office Hadley Centre (UK)	192×144
9	ACCESS-CM2	Commonwealth Scientific and Industrial Research Organisation, Australian Research Council Centre of Excellence for Climate System Science (Australia)	192×144
10	ACCESS-ESM1-5	Commonwealth Scientific and Industrial Research Organisation (Australia)	192×145
11	CanESM5	Canadian Centre for Climate Modelling and Analysis (Canada)	128×64
12	INM-CM4-8	Institute for Numerical Mathematics (Russia)	180×120
13	INM-CM5-0		180×120
14	EC-Earth3	EC-Earth-Consortium	512×256
15	MIROC6	Japan Agency for Marine-Earth Science and Technology/Atmosphere and	256×128

16	MIROC-ES2L	Ocean Research Institute/National Institute for Environmental Studies/RIKEN Center for Computational Science (Japan)	128×64
17	NorESM2-LM	NorESM Climate modeling Consortium consisting of CICERO (Norway)	144×96
18	KACE-1-0-G	National Institute of Meteorological Sciences/Korea Meteorological Administration (Korea)	192×144

Table 2 Parameters and performance of the GR4J model for the 7 calibrated watersheds (NSE, Nash–Sutcliffe efficiency; KGE′, modified Kling–Gupta efficiency; cal., calibration; val., validation)

Watershed code	**X_1 (mm)**	**X_2 (mm d^{-1})**	**X_3 (mm)**	**X_4 (day)**	**NSE (cal.)**	**NSE (val.)**	**KGE′ (cal.)**	**KGE′ (val.)**
1012	100.000	2.571	28.894	1.100	0.806	0.772	0.790	0.771
2015	230.147	1.317	26.785	1.158	0.857	0.785	0.929	0.822
2018	100.000	1.577	25.184	1.169	0.836	0.793	0.902	0.825
3001	100.000	1.360	22.164	1.100	0.810	0.747	0.892	0.794
4001	100.000	0.757	20.000	1.202	0.765	0.653	0.855	0.754
4007	146.844	−0.262	46.527	1.172	0.829	0.749	0.914	0.801
5101	1041.152	−5.000	27.347	1.150	0.736	0.668	0.868	0.732

Table 3 Selected marginal distributions and copula families of drought duration and severity by major river basin (GEV, generalized extreme value; LN, lognormal; GPD, generalized Pareto; WBL, Weibull)

Major river basin	Duration marginal		Severity marginal				Copula	
	GEV	LN	GEV	GPD	LN	WBL	Gumbel	Clayton
Han	23	7	0	11	15	4	21	9
Nakdong	30	3	8	7	18	0	33	0
Geum	19	2	3	2	13	3	21	0
Seomjin	15	0	2	3	10	0	15	0
Yeongsan	14	0	11	0	3	0	14	0
Total	**101**	**12**	**24**	**23**	**59**	**7**	**104**	**9**

Figures

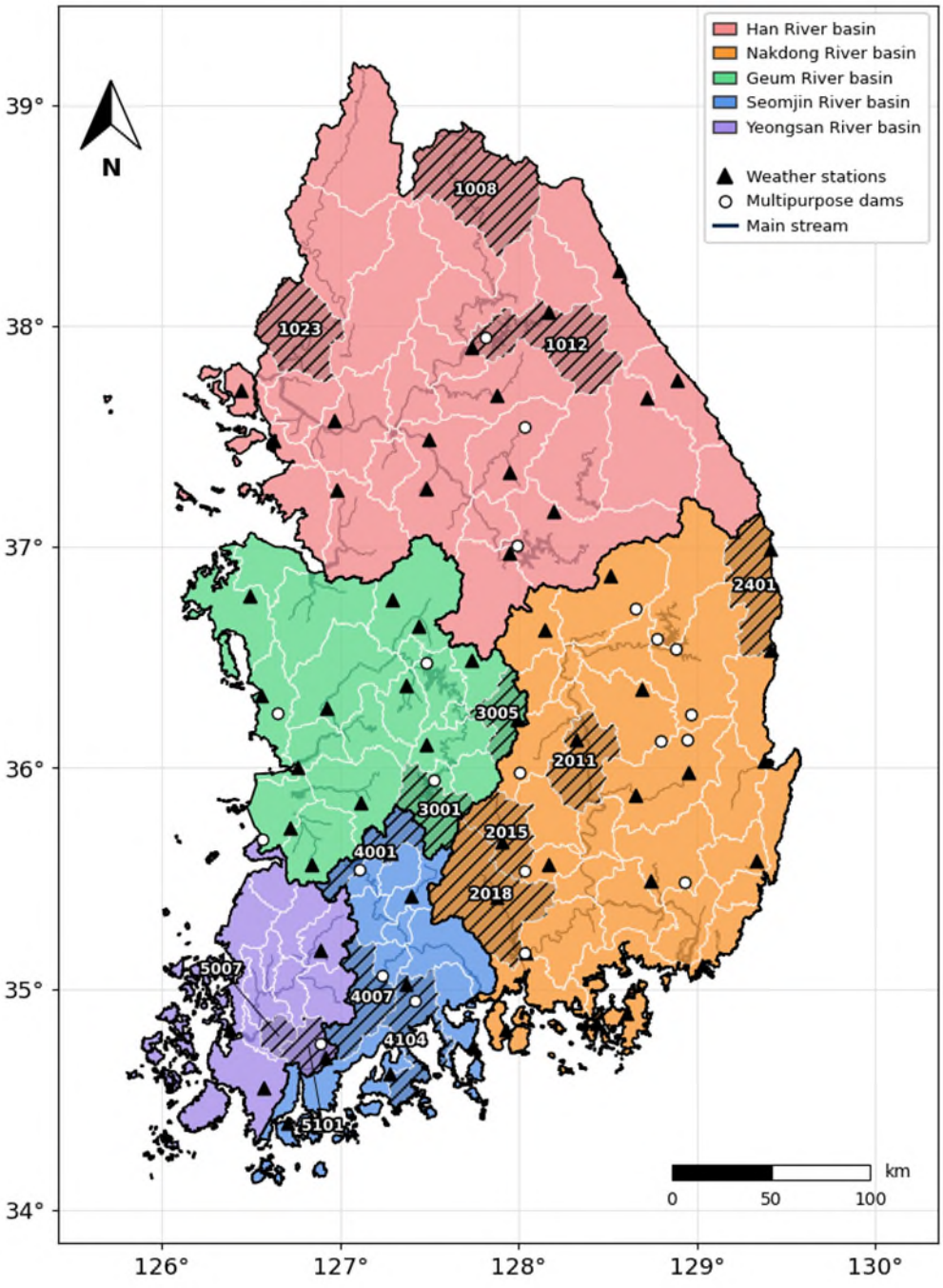


Fig. 1 Location of the 5 major river basins and 113 middle-sized watersheds in South Korea. Jeju, Ulleung, and Dokdo islands are excluded, and hatched watersheds indicate watersheds discussed in the manuscript

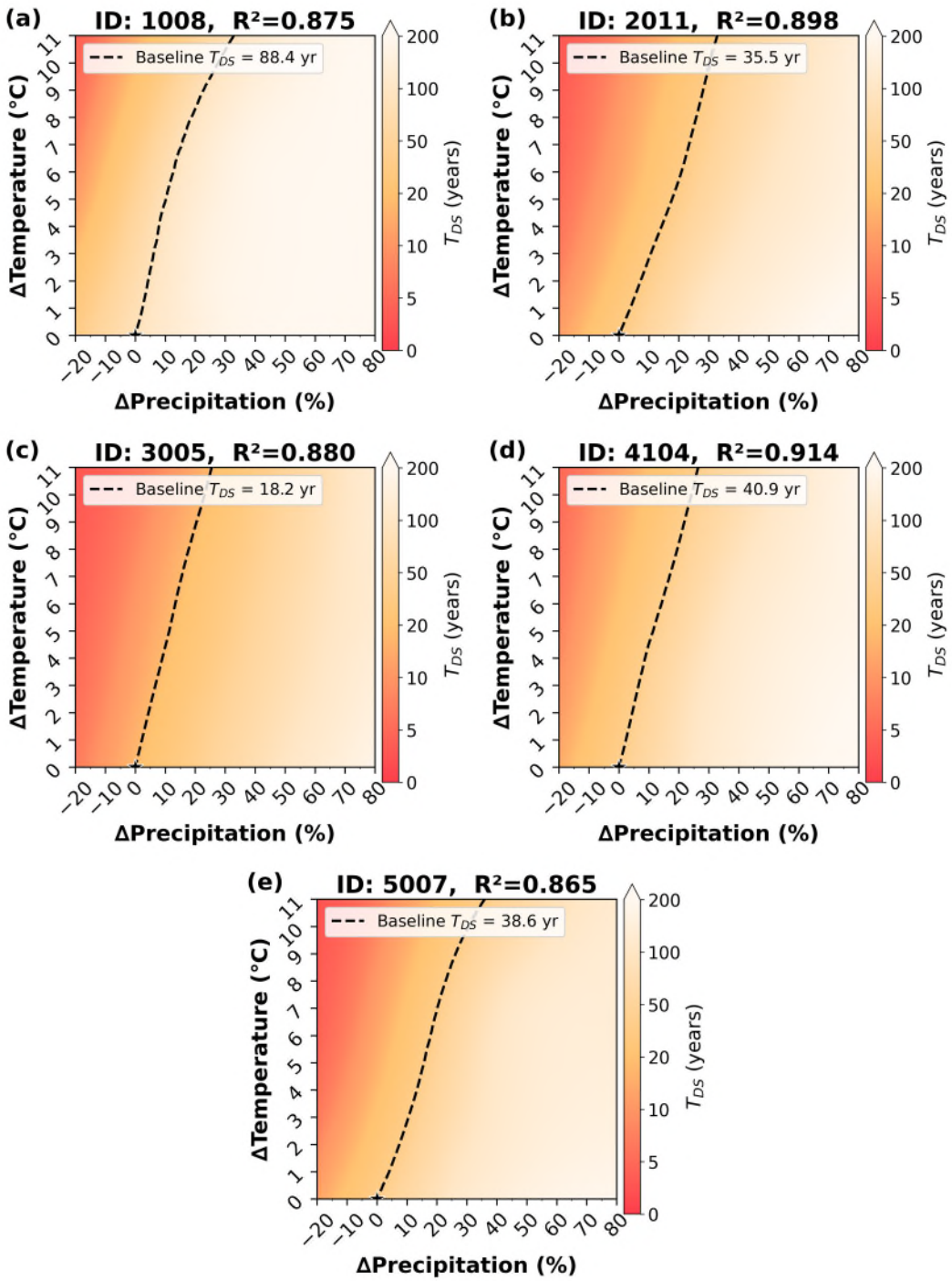


Fig. 2 Scenario-neutral response surfaces of the design drought return period (T_{DS}) for the representative watersheds selected from each major river basin

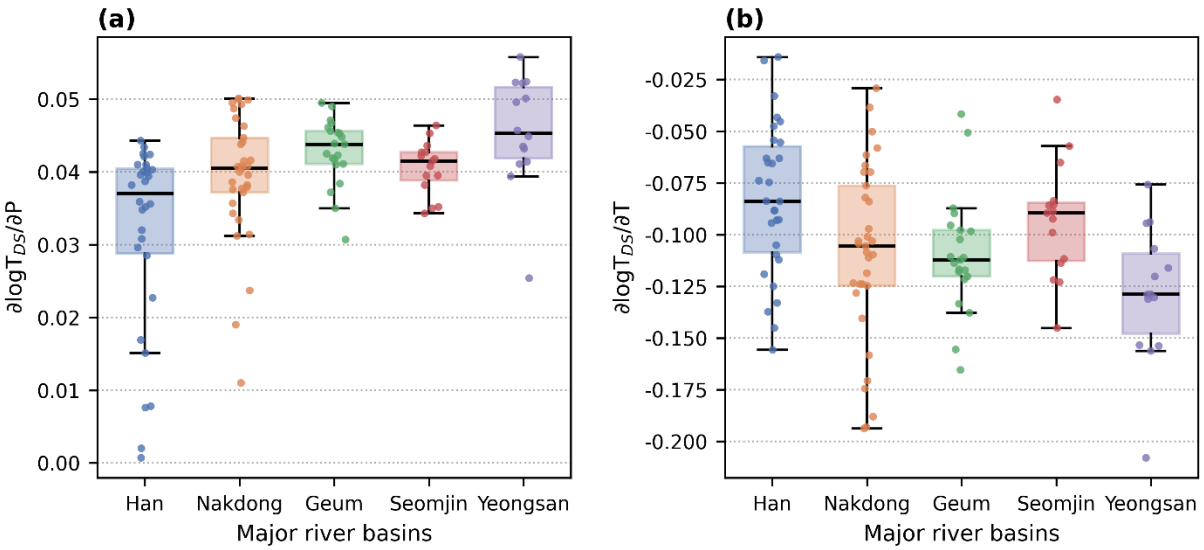


Fig. 3 Distributions of the response-surface sensitivities by major river basin: (a) precipitation sensitivity and (b) temperature sensitivity

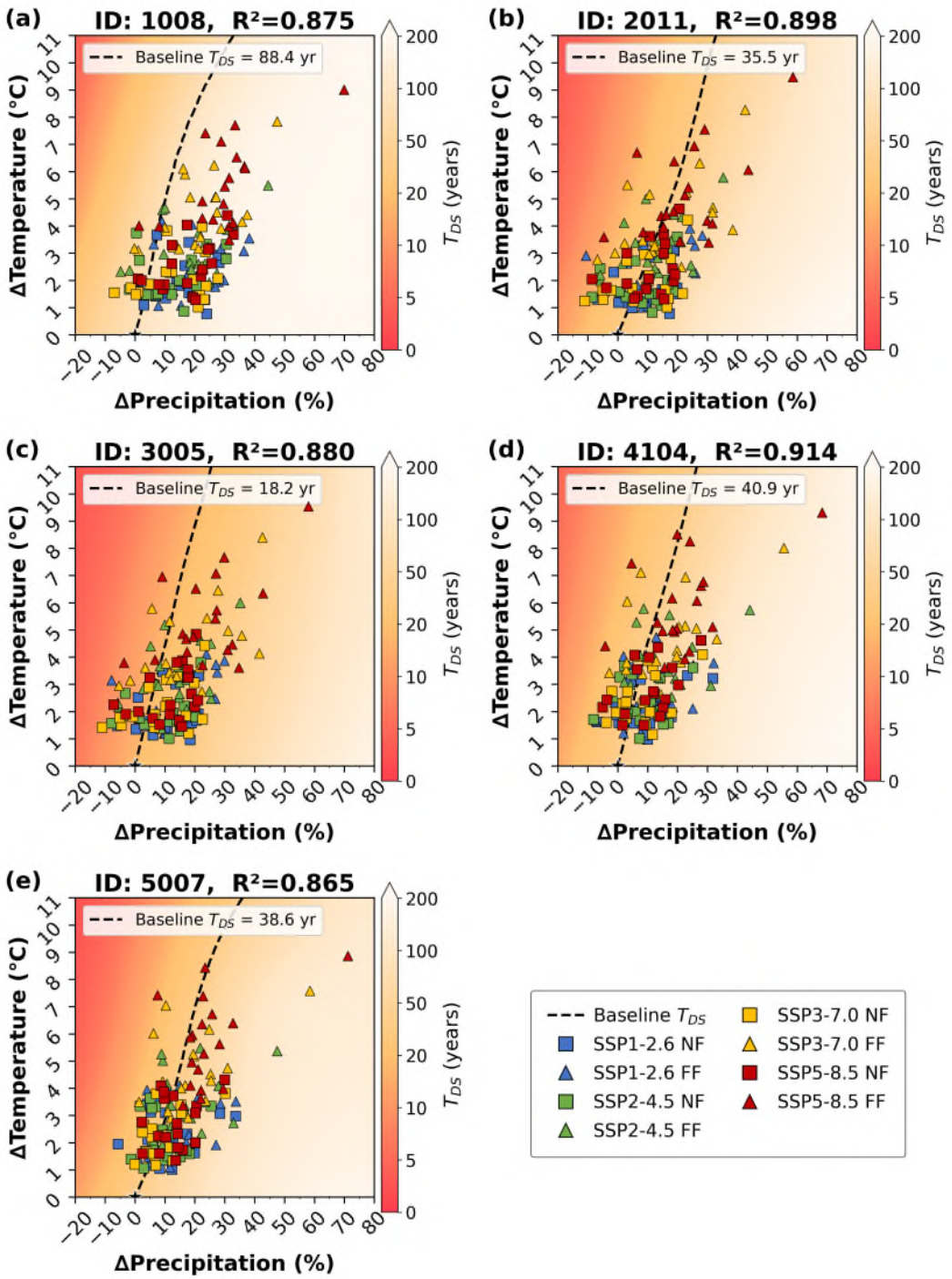


Fig. 4 SSP–GCM projections for the NF and FF overlaid on the scenario-neutral response surfaces for the representative watersheds selected from each major river basin